CHEMISTRY
A EUROPEAN JOURNAL

DOI: 10.1002/chem.200600780

Cathodic Electrografting of Versatile Ligands on Si(100) as a Low-Impact Approach for Establishing a Si–C Bond: A Surface-Coordination Study of Substituted 2,2′-Bipyridines with Cu^{I} Ions

Annalisa Aurora,[a] Fabrizio Cattaruzza,[b] Carlo Coluzza,[c] Claudio Della Volpe,[d] Giovanni Di Santo,[c] Alberto Flamini,[b] Carlo Mangano,[e] Simone Morpurgo,[a] Piersandro Pallavicini,*[e] and Robertino Zanoni*[a]

Abstract: Three distinct wet chemistry recipes were applied to hydrogen-terminated n- and p-Si(100) surfaces in a comparative study of the covalent grafting of two differently substituted 2,2′-bipyridines. The applied reactions require the use of heat, or visible light under a controlled atmosphere, or a suitable potential in an electrochemical cell. In this last case, hydrogen-terminated silicon is the working electrode in a cathodic electrografting (CEG) reaction, in which it is kept under reduction conditions. The resulting Si–C bound hybrids were characterized by a combination of AFM, dynamic contact-angle, and XPS analysis, with the help of theoretical calculations. The three distinct approaches were found to be suitable for obtaining ligand-functionalized Si surfaces. CEG resulted in the most satisfactory anchoring procedure, because of its better correlation between high coverage and preservation of the Si surface from both oxidation and contamination. The corresponding Si–bipyridine hybrid was reacted in a solution of CH_3CN containing Cu^{I} ions coordinatively bound to the anchored ligands, as evidenced from the XPS binding-energy shift of the N atom donor functions. The reaction gave a 1:2 Cu–bipyridine surface complex, in which two ligands couple to a single Cu^{I} ion. The surface complex was characterized by the Cu Auger parameter and Cu/N XPS atomic-ratio values coincident with those for pure, unsupported Cu^{I} complex with the same 2,2′-bipyridine. Further support for such a specific metal–ligand interaction at the functionalized Si surface came from the distinct values of Cu2p binding energy and the Cu Auger parameter, which were obtained for the species resulting from Cu^{I} ion uptake on hydrogen-terminated Si(100).

Keywords: monolayers · photoelectron spectroscopy · scanning probe microscopy · silicon · surface chemistry

Introduction

Molecular surface functionalization is an area under rapid development that extends into advanced fields of research, such as nanoelectronics, nanosensing, and biological interfaces at the nanoscale. Many efforts have been devoted to depositing monolayers of organic molecules on silicon-oriented surfaces.[1–11] The advantages of silicon as a substrate are numerous and its chemical reactivity has been widely explored. Silicon can operate as a semiconductor electrode, which facilitates applications of its functionalized surfaces in, for example, sensors and biosensors or, in the case of electroactive surfaces, charge-storage devices.[9–11]

Notably, few papers have addressed the issue of immobilization on Si(100) and Si(111) of molecules displaying any kind of function.[12–15] Grafting reactions of organic ligands have also been rarely reported.[16–18] So far, the rich redox, sensing, and switching chemistry offered by transition-metal complexes in solution appears almost completely unexploited in relation to the Si surface. Although the number of

[a] Dr. A. Aurora, Dr. S. Morpurgo, Prof. R. Zanoni
Dipartimento di Chimica
Università degli Studi di Roma "La Sapienza"
p. le A. Moro 5, 00185 Rome (Italy)
Fax: (+39) 06-490-324
E-mail: robertino.zanoni@uniroma1.it

[b] Dr. F. Cattaruzza, Dr. A. Flamini
CNR-ISM, Area della Ricerca di Montelibretti
C.P. 10, Monterotondo Stazione, 00016 Rome (Italy)

[c] Prof. C. Coluzza, Dr. G. Di Santo
Dipartimento di Fisica
Università degli Studi di Roma "La Sapienza" (Italy)

[d] Prof. C. Della Volpe
Università di Trento
Dipartimento di Ingegneria dei Materiali e Tecnologie Industriali
Via Mesiano 77, 38050 Trento (Italy)

[e] Dr. C. Mangano, Prof. P. Pallavicini
Dipartimento di Chimica Generale, Università degli Studi di Pavia
Via Taramelli 12, 27100 Pavia (Italy)
Fax: (+39) 0382-528-544
E-mail: psp@unipv.it

Supporting information for this article is available on the WWW under http://www.chemeurj.org/ or from the author.

such studies is surely limited because of the known reactivity of silicon towards oxidation in water, it does not explain the present lack of reports, even for less-reactive and less-widely investigated metal surfaces, such as Au(111).

The establishment of a carbosilane linkage (RC–Si), which is more robust than the alkoxysilane (RO–Si) anchoring group towards degradation in aqueous media under either acidic or basic conditions, is a surface modification with organic monolayers that is actively sought, because of the implied technological applications and also because it enables the study of chemical and electronic processes at the semiconductor surface. The methods reported make use of Grignard reagents (both on preliminarily halogenated Si surfaces and through anodic electrografting),[19,20] aryldiazonium salts,[21,22] Lewis acids,[23] diacyl peroxides,[24,25] alkyl halides,[26] alkenes,[4,12,25,27–30] and alkynes.[25,31–38] Although, in principle, each of the above precursors and methods are suitable for academic research, some are far indeed from what industry could be willing to adopt. A comparative evaluation of the pros and cons of specific routes should be conducted on suitable molecules, or even on different functional groups.

We recently explored three distinct series of functional molecules as test reagents for the comparison and optimization of wet chemistry anchoring procedures on Si. These series differ in the presence of specific terminal groups that are able, upon further reaction, to 1) generate new covalent bonds, 2) produce electroactive surfaces, 3) form surface-coordination complexes.

Series 1 is represented by COOH-terminated organic monolayers on Si(100), which can act as the substrate for the anchoring of protein,[39] oligonucleotides,[40] and, as recently demonstrated by some of us, magnetic nanoparticles[41] and fluorescent probes.[35] This last system was produced by heat- or visible-light-promoted functionalization and through a cathodic electrografting (CEG) reaction.[42] CEG provided the better procedure, in which both a larger surface coverage and a smaller impact on Si surface oxidation were obtained.[35]

Monolayers of substituted ferrocenes are examples of series 2. For selected derivatized ferrocenes, anchored through Si–C or Si–O bonds, a photochemical reaction with visible light from low-melting-point precursors was shown to be superior to thermal initiation, both for its much reduced impact on the initial H–Si surface and for the better electrical characteristics of the redox-active hybrid.[4,14]

Series 3, the least-explored one, is the object of the present report, in which the preparation and coordination properties of covalently bound monolayers of 2,2′-bipyridine ligands on Si were studied. These very popular ligands[43] belong to a series of polybidentate species with sp^2-hybridized N atom donors, and have demonstrated both electrochemical bistability and hysteresis upon coordinating Cu ions in solution.[44] These properties suggest their possible use for data storage at a molecular level. Further investigations of the surface-coordination properties on Si of pH-switchable polyamino–polyamido ligands, which are able to uptake/release and translocate one or two Cu^{2+} cations, are underway.[45]

Experimental Section

General: Functionalization experiments on the surface-activated samples were carried out in a N_2(g)-purged dry-box (Braun) or by using standard preparative Schlenk-line procedures. An AMEL system (Model 550 Potentiostat and Model 721 Integrator) was used for the electrochemical experiments. Si(100) wafers of ~400 μm thickness, p-Si (boron-doped, single-side polished, 1–10 Ω cm resistivity) and n-Si (phosphorus-doped, single-side polished, 0.007–0.013 Ω cm resistivity) were purchased from Si-Mat. 5-Vinyl-2,2′-bipyridine and 5-bromomethyl-2,2′-bipyridine were prepared according to literature procedures.[46] Commercial (Fluka) tetraethylammonium perchlorate (TEAP) was dried at 65 °C under vacuum. Acetonitrile (CH_3CN) was carefully dried and freshly distilled over CaH_2 before use. Copper(I) tetrakis-acetonitrile perchlorate, [Cu(CH_3CN)$_4$]ClO_4, was prepared as reported in the literature.[47]

Preparation of hydrogenated silicon: Si(100) wafers with areas of about 1 cm^2 were initially washed in boiling 1,1,2-trichlorethane for 10 min and subsequently in methanol at RT, with sonication for 5 min. They were then oxidized in H_2O_2/HCl/H_2O (2:1:8) at 353 K for 15 min, rinsed copiously with water, etched with 10% aqueous HF for 10 min, rinsed with water again, dried under a stream of N_2, and immediately used in the functionalization process in a dry-box. The main steps of the procedure were taken from the literature.[48]

Monolayer preparation on silicon: Several samples were prepared, according to the different routes described below. Freshly etched Si samples were used throughout. After functionalization, all samples were subjected to the same cleaning procedure, consisting of four sonication cycles, 5 min each, with different solvents (toluene, acetonitrile), then dried in a stream of N_2.

Photoimmobilization (*hν*): A hydrogen-terminated Si(100) wafer was placed in a levelled Petri dish inside the dry-box, covered with neat 5-vinyl-2,2′-bipyridine, and then subjected to irradiation with visible light at 35 mW cm^{-2} for 1 h from a quartz/iodine lamp, while being heated slightly above the melting point of 5-vinyl-2,2′-bipyridine (~50 °C).

Thermal immobilization (Δ): Neat 5-vinyl-2,2′-bipyridine was placed on the surface of a hydrogen-terminated Si(100) wafer in a stoppered tube under N_2, heated to above its melting point, and then allowed to react at this temperature for 1 h.

Electrografting (CEG): The electrografting preparation route, derived in part from the literature,[26] was carried out at a constant cathodic-current density of 10 mA cm^{-2} for 2 min, without illumination, in a two-compartment polyethylene cell, placed inside the dry-box. The working electrode was a hydrogenated n-Si wafer with a diameter of 2.54 cm, exposing a 1.5 cm^2 area, in a solution of the reactant (5-bromomethyl-2,2′-bipyridine, 0.1 M) and the supporting electrolyte (TEAP, 0.1 M) in CH_3CN (3.5 cm^3). A similar procedure was used for the electrografting functionalization of p-Si(100). In both cases, an ohmic contact on the rear side of the silicon wafer was obtained with an In/Ga eutectic mixture. The counterelectrode was a Pt wire immersed in a solution of TEAP (0.1 M) in CH_3CN (3 cm^3) filling a glass tube, separated from the working compartment by a glass sintered disc (porosity 3).

Preparation of the Cu^I complex with a bipyridine-functionalized Si(100) surface: A Si(100) wafer, immediately after electrochemical grafting with 5-bromomethyl-2,2′-bipyridine, was soaked with ethanolic or acetonitrile solutions (0.1 M) of $Cu(CF_3SO_3)_2$ or [Cu(CH_3CN)$_4$]ClO_4, respectively, for 2 min, inside the dry-box. The sample was eventually removed from the dry-box and then thoroughly washed in air by using the cleaning procedure described above.

AFM: A needle-sensor atomic force microscope (VT-AFM, Omicron NanoTechnology) was used. The silicon nitride microfabricated tips, with a nominal curvature radius of ~10 nm, showed a resonance frequency of 997.500 Hz. Rms roughness (defined as the standard deviation with re-

spect to the average height) and average height values were calculated by using the Scala Pro routines (Omicron NanoTechnology). The images were processed by WSxM 3.0 Beta 2.3 scanning probe microscopy, free software available from Nanotec Electronica SL. The height distributions were calculated by using Gwyddion 1.12, a free software covered by GNU General Public Licence. All images are shown with their associated maximum and minimum z values, reported in the corresponding look-up tables.

X-ray photoelectron spectroscopy: XPS results were obtained by using an experimental apparatus in ultrahigh vacuum (UHV) consisting of a modified Omicron NanoTechnology MXPS system, with an XPS chamber equipped with a dual X-ray anode source (Omicron DAR 400) and an Omicron EA-127 energy analyzer, and an attached VT-atomic force and scanning tunneling microscope. Sample transfer between the various experimental areas was conducted by means of linear magnetic transfer rods or manipulators. All measurements were recorded as soon as possible after sample preparation. Samples were produced and mounted on sample holders in a dry-box, transferred from the dry-box to the XPS facility in Schlenk tubes, under N_2. They were then introduced into the XPS chamber after being exposed to air for about 1 min. No significant sample degradation under extended acquisition times under the X-rays was observed. $Mg_{K\alpha}$ and $Al_{K\alpha}$ photons were employed ($h\nu = 1253.6$ and 1486.6 eV, respectively), and the anode was operated at 14–15 kV, 10–20 mA. No charging was experienced by the hybrid species, as can be inferred from the coincidence of the binding energy (BE) for the $Si2p_{3/2}$ bulk component peak position with the value of 99.7 eV, taken from the literature.[49] BE values were derived from experimentally determined kinetic energies (KE) from the relation: $BE = h\nu - KE$, after spectrometer energy calibration with metal standards. XPS atomic ratios for the bipyridine-functionalized hybrids were estimated from experimentally determined area ratios of the relevant core lines, corrected for the corresponding theoretical atomic cross-sections and for a square-root dependence of the photoelectron kinetic energies. The effects on quantitative analysis possibly generated by XPS measurements from oriented Si wafers because of photoelectron diffraction at preferential directions of electron collection[50] were minimized by mounting the Si(100) wafers always with the same orientation with respect to the analyzer axis. All reported spectra were acquired at a photoelectron take-off angle of 11°, measured from the surface normal.

Theoretical investigations: The large dimensions of the systems under investigation suggested the use of a monohydride-type surface termination for Si(100), even if a mixture of mono-, di- and trihydride was experimentally found for similarly obtained surfaces. All calculations were performed by using the Gaussian 98 package.[51] The bonding of 5-methyl-2,2′-bipyridine to the monohydrogenated Si(100) surface was simulated by using the model cluster $Si_{13}H_{18}$, in which dangling bonds were saturated by hydrogen atoms. Because of the relevant dimensions of such systems, geometry optimizations were performed at the HF/3-21G level. All optimized structures were vibrationally characterized to check for the absence of imaginary frequencies in the minima and to compute zero-point energy (ZPE). ZPE values calculated at the HF/3-21G level were scaled by a factor of 0.91, which is commonly employed to correct harmonic frequencies computed at the HF-level.[52,53] Single-point calculations at the B3LYP/6-31G*//HF/3-21G level were performed to derive the relative energy of isomeric structures and for electronic-structure analysis. Mulliken analysis[54] was not very reliable for the system under investigation and the fraction of electronic charge located on each atom was derived instead by distributed multipole analysis (DMA).[55,56] The latter method is implemented in the molecular visualization MOLDEN[57] program.

Dynamic contact angles (DCA): Contact angles were measured by using the Wilhelmy method with a microbalance CAHN 322 thermostated at 20 ± 0.5 °C. The immersion speed was 20 μm sec^{-1}. The different solvents used were MilliQ-grade water, ethylene glycol (99 %), and 1-bromonaphthalene (97 %) (Sigma). Electrochemical grafting does not give double-sided functionalization. All measurements were performed by cutting each original sample into two equal halves and suitably gluing them to leave the functionalized surface outside. The surface free energy, γ_{total}, and components γ_+, γ_-, and γ_{LW}, were calculated by using literature methods,[58,59] with the help of an in-house-developed program, which can be freely accessed (http://www.ing.unitn.it/~devol). Details of the method have been reported elsewhere.[60]

Results

The characterization of H–Si(100) surfaces is reported below, followed by the XPS and AFM results from covalent grafting on H–Si(100) of the substituted 2,2′-bipyridines. The anchoring reactions were conducted by using visible light ($h\nu$) or heat (Δ), or through cathodic electrografting (CEG), and two different precursors were used, 5-vinyl-2,2′-bipyridine and 5-bromomethyl-2,2′-bipyridine, depending on the recipe used for grafting (Figure 1, paths a–c). On the hybrid of choice, the experimental and theoretical characterization of the species resulting from its reaction with Cu^I ions from a CH_3CN solution are presented.

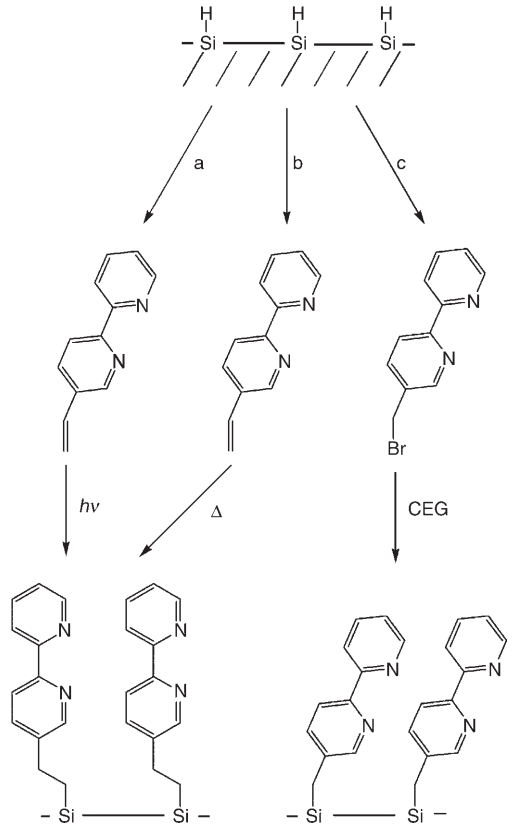

Figure 1. Different synthetic approaches used for hydrogen-terminated Si(100) functionalization with bipyridines, and their resulting species: path a: photochemical reaction of 5-vinyl-2,2′-bipyridine; path b: thermal reaction of 5-vinyl-2,2′-bipyridine; path c: wet chemistry synthesis through cathodic electrografting of 5-bromomethyl-2,2′-bipyridine.

Hydrogen-terminated surfaces: The average values found for advancing/receding contact angles of H–Si(100) surfaces in water were 80/40°, with a notable hysteresis in all three

solvents used, as evidenced in Table 1. The advancing angles in all cases decrease as the liquid surface tension decreases. The receding angles approach zero for ethylene glycol, which has an intermediate value of surface tension, probably indicating a specific interaction. With 1-bromonaphthalene, the closely comparable values for advancing and receding angles indicate the formation of a stable film of solvent molecules on the surface. Table 2 shows the advancing/receding free energies that were calculated by using the dynamic contact angles presented in Table 1.

Table 1. Average advancing/receding dynamic contact angles in different solvents [°]. The associated standard deviations are within ±1–2°. The CEG sample was obtained from cathodic electrografting of 5-methyl-2,2′-bipyridine to hydrogenated p-Si(100). CEG sample + Cu^{I} is the sample resulting from exposure of a CEG sample to a solution of Cu^{I} ions in CH_3CN.

	Water	Ethylene glycol	1-Bromonaphthalene
H-terminated Si(100)	80/40	51/0	31/21
CEG sample	73/17	49/12	24/17
CEG sample + Cu^{I}	83/43	56/24	51/51

Table 2. Advancing/receding surface free energies (γ_{total}) and distinct components [mJ m^{-2}] calculated from the values for advancing/receding dynamic contact angles and estimated by using the acid–base approach. Standard deviations are within ±1–3 mJ m^{-2}.

	γ_{total}	γ_{LW}	γ_+	γ_-
H-terminated Si(100)	40/50	39/41	0/0	7/36
CEG sample	42/46	41/43	0/0	11/61
CEG sample + Cu^{I}	33/44	29/30	0.5/1.4	6/39

Application of in situ AFM allowed the assessment of the surface morphology at the various reaction steps. AFM images taken from n- and p-doped hydrogen-terminated Si(100) surfaces are reported in Figure 2a and b, respectively. They are representative of the total area explored. Very low and comparable values of rms roughness were found for both n- and p-doped samples.

XPS results from the relevant core regions of Si, C, and O revealed the absence, within the present experimental limits, of silicon oxide and the presence of some residual C and O contamination. The latter could have resulted from the short exposure to air, which was necessary to transport the samples from a dry-box, in which the preparation was conducted, to the UHV apparatus. Si2p generates a complex peak, from which a distinct component, at a binding energy (BE) 0.4 eV larger than the main spin-orbit doublet at 99.7 eV, can be assigned to the reacted Si surface atoms. The relative shift of the components to the main peak is fully compatible with the expected silicon dihydride termination, although minor contributions from mono- or trihydrides can easily escape detection. Some residual intensity on the low-BE side, barely visible in the XPS spectrum, was attributed to surface defects.[4]

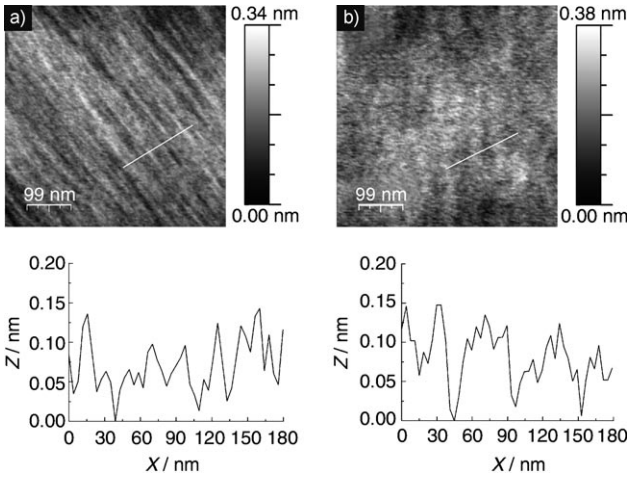

Figure 2. Top: AFM images (500×500 nm^2) from a) n-Si(100)–H and b) p-Si(100)–H clean substrates. Bottom: corresponding linear cross-section profiles taken along the segments marked by the white lines (top). The rms roughness values are 0.06 and 0.05 nm, respectively.

Functionalized Si surfaces: A detailed comparison of the three recipes for bipyridine grafting on hydrogen-terminated Si(100) was conducted by XPS, which allows the simultaneous elucidation of both the state of the surface, in terms of the presence of oxide and/or contaminants, and the extent of functionalization, through relative quantitative measurements from intensity ratios of core lines.

Percent-coverage values for the hybrids, inferred from XPS, are plotted against silicon oxide thicknesses in Figure 3, and the experimental and curve-fitted core lines are collected in Figure 4 (see also Table S1 of the Supporting Information).

Experimental determination of the SiO_2 thickness was achieved by using a surface quantitative model taken from the literature,[48,49,61] which leads to Equation (1):

$$d_{ox} = L_{SiO_2}(E_{Si}) \cos\theta \ln(1 + R_{exp}/R_o) \quad (1)$$

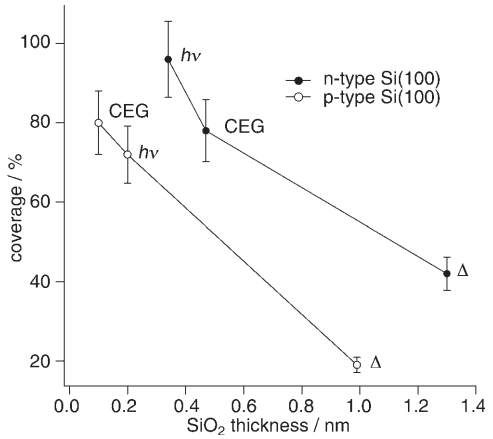

Figure 3. Plot of the percentage coverage values versus SiO_2 thickness for n- and p-Si(100) surfaces functionalized with substituted bipyridines by different routes. CEG, *hν*, and Δ have the same meanings as in Figure 1. The solid lines are traced to guide the eye.

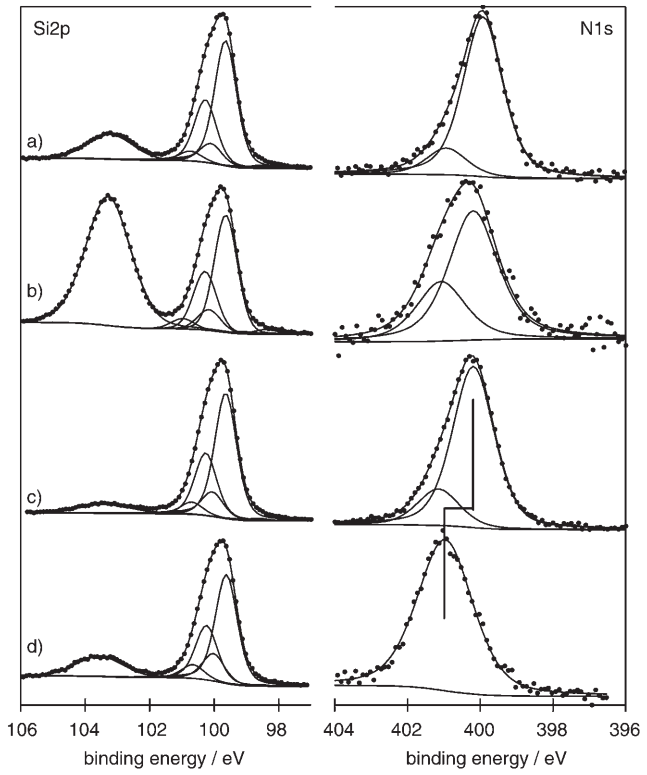

Figure 4. N1s and Si2p XPS spectra for hydrogen-terminated n-Si(100) after the following treatments: a) photochemical grafting of 5-vinyl-2,2′-bipyridine (consistently similar spectra are obtained from thermal anchoring); b) thermochemical grafting of 5-vinyl-2,2′-bipyridine; c) cathodic electrografting of 5-bromomethyl-2,2′-bipyridine; d) cathodic electrografting of 5-bromomethyl-2,2′-bipyridine, followed by immersion in a 0.1 M solution of $[Cu(CH_3CN)_4]ClO_4$ in acetonitrile.

in which d_{ox} is the total oxide thickness (nm) due to the four different Si_xO_y species, $L_{SiO_2}(E_{Si})$ is the attenuation length of Si2p photoelectrons from SiO_2, θ is the collection angle of the photoelectrons taken from the surface normal, R_{exp} is the measured $I_{silica}/I_{silicon}$ ratio, and R_o is the $I_{silica}/I_{silicon}$ ratio for the pure species. The product $L_{SiO_2}(E_{Si})\cos\theta$ is the inelastic mean-free-path of Si2p photoelectrons. It is recalled here, as a reference, that one monolayer of silica grown on silicon is 0.35 nm thick. The total oxide thickness is obtained from the application of Equation (1) and is a quantitative estimate of a continuous overlayer. Very small values (<0.35 nm) indicate that the surface oxidation is limited to very small areas. The values in Figure 3 allow for a clear distinction to be made between the preparation routes.

In the modified substrates, the appearance of the characteristic N1s peak in the XPS spectra indicates the presence of the molecular moiety. The coverage values, reported in Figure 3, were calculated from the ratio of the normalized peak intensities of N1s, I_{N1s}, to Si2p, I_{Si2p}, according to Equation (2):[62]

$$\Phi = (I_{N1s}/n\sigma_{N1s})(\sigma_{Si2p}/I_{Si2p})(AF_{ml}/IF_{Si(100)}) \quad (2)$$

in which AF_{ml} is the attenuation factor associated with the presence of a surface monolayer ($AF_{ml}=\exp[-d_{ml}/L_{ml}(E_{ml})\cos\theta]$), $IF_{Si(100)}$ is the intensity factor for unattenuated silicon, $IF_{Si(100)}=1-\exp[-d_{Si}/L_{Si}(E_{Si})\cos\theta]$, and n is the number of nitrogen atoms of the molecule. The layer spacing, $d_{Si(100)}$, and the inelastic mean-free-path values for both silicon, $L_{Si}(E_{Si})$, and the monolayer, $L_{ml}(E_{ml})$, were taken from the literature.[63–65] The monolayer thickness, d_{ml}, was deduced from DFT calculations; the cross-section values, σ, for N1s and Si2p were taken from Scofield.[66]

The ionization region for N1s presents different components in the corresponding three series. In all cases, the curve-fitting of N1s shows an intense component at a BE of 399.8 eV, which can be confidently assigned to the N atom functions in the neutral 2,2′-bipyridine moiety, on the basis of closely comparable literature BE values for differently substituted pyridines.[67,68] A second common feature, located at ~401 eV, was assigned with the help of results from theoretical calculations, as discussed in the next section.

In the CEG samples, the C1s/N1s XPS atomic ratio was close to the theoretical value of 5.5. More-extensive carbon contamination was detected for samples obtained from thermal and photochemical treatments. Analogously, some oxygen-related contamination was inferred from the O1s/Si2p ratio, higher than the value expected on the basis of the amount of silica.

The formation of a stable Si–C covalent bond was indirectly confirmed in the three series of samples by treating the hybrids in aqueous NaOH (0.1 M) solution for 2 min. XPS analysis of the resulting surface proved that the relevant molecular ionization peaks survived the treatment.

AFM images were recorded from the hybrids resulting from all three treatments. CEG sample surfaces revealed a homogeneous morphology, consisting of globular assemblies. Figure 5 shows AFM images of the CEG sample at different frame enlargements, and linear cross-section profiles taken from a measured area of 7.1×7.1 μm^2. Structures resembling elongated grains, distributed without a long-range order, are clearly visible. In the enlarged views, reported in Figure 5b and c, the ~20×30 nm^2 grains appear with regular shapes and are laterally separated by 20–30 nm. The rms roughness value obtained from these images is 0.56 nm. The height distribution evaluated from statistical analysis of AFM images shows that the average height of the grains is 0.822 ± 0.003 nm, however, for the samples resulting from thermal and photochemical procedures, a broader distribution results, peaking at ~3.2 nm, with an rms roughness value of ~1.2 nm (see Figure S1 of Supporting Information).

Dynamic contact-angle values of the CEG sample were analyzed, and the average values for advancing/receding angles are summarized in Table 1. An hysteresis between advancing and receding curves was identified and was attributed to surface reactivity because of Si oxidation. This was further confirmed by observing a decrease in the values upon subsequent immersions of the same sample. Relative to the hydrogen-terminated surface, the CEG sample shows lower values of contact angle (73/17°), which is in accord

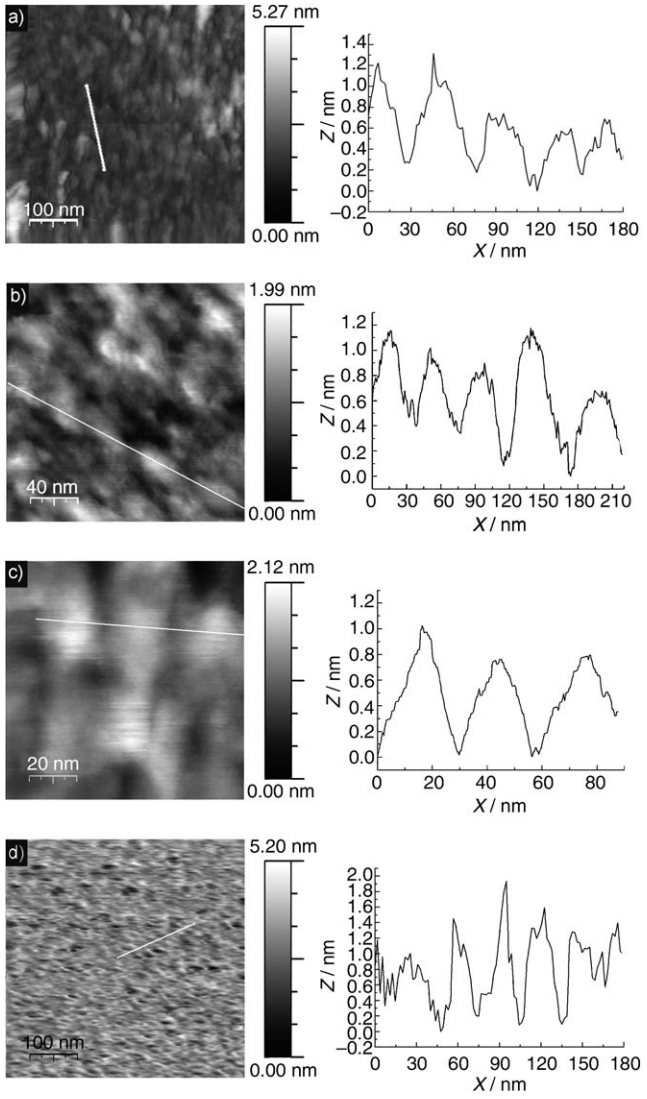

Figure 5. a) AFM image ($500\times500\ nm^2$) of a freshly prepared CEG sample on p-Si(100) obtained from cathodic electrografting of 5-bromomethyl-2,2′-bipyridine on p-Si(100) (left), and a cross-section profile from the same area (right); b) and c) close-up views (200×200 and $100\times100\ nm^2$, respectively) (left), and linear cross-section profiles (right) of the area shown in the AFM image in Figure 5a; d) AFM image ($500\times500\ nm^2$) from a freshly prepared CEG sample on p-Si(100) and coordinated with Cu^I (left), and a cross-section profile from the same area (right).

with the presence of electron donor or basic portion introduced on the surface by the bipyridine moiety.[69]

Theoretical calculations were undertaken to elucidate the main experimental findings and to model the surface-bound ligand and the Cu^I complex. Preliminary calculations were performed to define the molecular properties of the free bipyridines, which mainly exist as *syn* and *anti* rotamers, with reference to the reciprocal N atom position. The relative ring orientation is conventionally indicated by the ϕ (N1′-C2′-C2-N1) dihedral angle. At the B3LYP/6-31G* level, the *anti* rotamer ($\phi=180°$) is favored over the *syn* rotamer ($\phi\sim35°$) by $\sim6.7\ kcal\,mol^{-1}$ in free bipyridine. Protonation of one of the ligand N functions inverts the relative stability, with the *syn* rotamer ($\phi=0°$) being favored by $\sim7.4\ kcal\,mol^{-1}$, the added stability coming from the $NH^+\cdots N$ interaction. The introduction of a SiH_3–CH_2– anchoring arm in the bipyridine frame does not modify the above order. Further calculations, giving the data reported in Table 3 and Figure 6, were aimed at modelling bipyridine anchored to Si(100) through a CH_2 group in the ring position 5.

Structure **1** in Table 3 (Figure 6a) represents the *anti* rotamer of 5-methyl-2,2′-bipyridine bonded to the Si(100) surface. Structures **2** and **3** represent the *syn* rotamers, which differ from each other in the orientation of the distal pyridine ring with respect to the proximal one ($\phi=\pm35°$). The structures indicated as **4**–**7** represent monoprotonated 5-methyl-2,2′-bipyridine bonded on the Si(100) surface. In all cases, the relative stability order (Table 3) is closely consistent with that calculated for the isolated analogues, and the angle between the plane of the proximal pyridine ring and the surface is nearly 48°. The distance between the farthest carbon atom of 2,2′-bipyridine and the Si(100) surface is about 0.83–0.84 nm.

Further calculations were undertaken in which the oxidized Si(100) surface was simulated by using the $Si_{13}H_{18}$ cluster with one of the hydrogen atoms replaced by an OH group. In structure **8**, the OH group and 5-methyl-2,2′-bipyridine (the *anti* rotamer is considered here) are both bonded to the Si atoms of the central dimer in the cluster. In this case, only a relatively long (0.24 nm) and weak OH···N hydrogen bond is formed, which does not change the orientation of 2,2′-bipyridine with respect to the surface. In **9**–**11**, the OH group is bonded to a Si atom of the nearest Si–Si dimer. The hydrogen bond between Si–OH and the nitrogen atom of *anti*-2,2′-bipyridine involves the proximal ring in **9** (Figure 6b) and the distal ring in **10**. In **11**, the OH group is hydrogen bonded to the N atom of the distal ring of *syn*-2,2′-bipyridine. The latter structure was also obtained if geometry optimization began with the OH group that is hydrogen bonded to the N atom of the proximal ring.

A common feature of **9**–**11** is that, in all cases, 5-methyl-2,2′-bipyridine is side-bent on the surface, suggesting that the presence of a methylenic group in the 5 position adds sufficient flexibility to the bipyridine moiety. Hydrogen bonding to silanol groups, however, reduces the distance to the surface of the farthest carbon atom to ~0.70 nm. The **9**–**11** structures show stronger hydrogen bonds than **8**, with shorter OH···N distances (0.183–0.188 nm).

The order of stability of the above structures reflects the higher stability of isolated *anti*-2,2′-bipyridine. However, **11** is less stable than **9** by only $3.4\ kcal\,mol^{-1}$. Comparison of such a value with the energy difference between *anti* and *syn* rotamers of isolated 2,2′-bipyridine shows that **11** is the structure with the strongest hydrogen bond.

The net atomic charges are also reported in Table 3. Surface binding (structures **1**–**3**) does not result in any difference between the charges on the N atoms of 2,2′-bipyridine. For monoprotonated 2,2′-bipyridine, the difference between the charges of N atoms is 0.3–0.4 for the *anti* rotamers

Table 3. Computational results obtained for 5-methyl-2,2′-bipyridine (bp) bonded on a Si(100) cluster (CL):[a] B3LYP/6-31G*//HF/3-21G electronic energy (E_{el}/a.u.), zero-point energy (ZPE/a.u.), relative energy (E_{rel}/kcal^{-1}mol^{-1}), electronic charge fraction (q_i/a.u.) located on N1 and (see text and Figure 6) calculated according to Mulliken[53] or by distributed multipole analysis (DMA),[54,55] and DMA charge difference (Δq_i/a.u.) between the nitrogen atoms of 5-methyl-2,2′-bipyridine.

	System	E_{el}	ZPE	E_{rel}	q_i (Mulliken)[b]		q_i (DMA)[b]		Δq_i (DMA)[c]
					N1	N1′	N1	N1′	
	pyridine[d]				−0.41		−0.62		
	pyridinium ion[d]				*−0.45*		*−0.09*		
1	CL−CH_2bp (*anti*)	−4307.86024	0.32185	0.00	−0.50	−0.50	−0.55	−0.56	0.01
2	CL−CH_2bp (*syn*)[e]	−4307.84994	0.32126	6.09	−0.45	−0.45	−0.64	−0.62	0.02
3	CL−CH_2bp (*syn*)[f]	−4307.85000	0.32126	6.05	−0.45	−0.45	−0.63	−0.65	0.02
4	CL−CH_2bpH$^+$ (*syn*)	−4308.25915	0.33570	0.00	*−0.62*	−0.55	*0.03*	−0.55	0.58
5	CL−CH_2bpH$^+$ (*syn*)	−4308.25695	0.33564	1.34	−0.55	*−0.61*	−0.56	*0.08*	0.64
6	CL−CH_2bpH$^+$ (*anti*)	−4308.24744	0.33557	7.26	*−0.65*	−0.49	*−0.20*	−0.53	0.33
7	CL−CH_2bpH$^+$ (*anti*)	−4308.24519	0.33548	8.63	−0.50	*−0.65*	−0.51	*−0.10*	0.41
8	CL−CH_2bpOH (*anti*)	−4383.12475	0.32798	2.53	*−0.51*	−0.50	*−0.51*	−0.56	0.05
9	CL−CH_2bpOH (*anti*)	−4383.13089	0.33009	0.00	*−0.57*	−0.50	*−0.29*	−0.58	0.29
10	CL−CH_2bpOH (*anti*)	−4383.12710	0.32931	1.89	−0.48	*−0.55*	−0.57	*−0.38*	0.19
11	CL−CH_2bpOH (*syn*)	−4383.12463	0.32923	3.39	−0.47	*−0.52*	−0.56	*−0.18*	0.38
12	CL−CH_2CH_2bp (*anti*)	−4347.17446	0.38444	0.0					
13	CL−CH_2CHbp (*anti*)	−4347.15688	0.38182	9.4					
14	CL−CH=Cbp (*anti*)	−4345.94163	0.35668	}25.2					
	H_2	−1.17544	0.01060						
15	CL−Cu^I(5-methyl-2,2′-bipyridine)$_2$	−2630.98749	0.31824	–	0.72 (Cu)	−0.64 (N)	−1.05 (Cu)	0.33 (N)	

[a] CL = $Si_{13}H_{17}$ cluster for **1–7**, **12**, **15**; $Si_{13}H_{18}$ for **13–14**, and $Si_{13}H_{16}OH$ for **8–11**. [b] The q_i charge located on protonated or hydrogen-bonded N atoms is reported in italics. [c] $\Delta q_i = |q_{N1} - q_{N1'}|$. [d] Geometry optimization at the B3LYP/6-31G* level. [e] (N1′-C2′-C2-N1) dihedral angle = −34.4°. [f] (N1′-C2′-C2-N1) dihedral angle = 34.4°.

(structures **6** and **7**) and 0.6 for the *syn* rotamers (structures **4** and **5**). Hydrogen bonding in **9–11** results in charge differences on the N atoms in the range of 0.19–0.38.

The structures **12–14** (Figure 6) were optimized to investigate how 5-ethyl-2,2′-bipyridine is bonded to the Si(100) surface. The ethyl group in **12** is bonded to the Si surface by only the proximal C atom, whereas in **13** both C atoms of the ethyl group are bonded to a surface Si dimer. In the latter structure, the Si−Si bond is broken and both Si atoms are hydrogenated. The structure of **14**, in which the molecular moiety is 5-ethenyl-2,2′-bipyridine, can be obtained by dehydrogenation of **13** and implies the formation of a C=C double bond. As shown in Table 3, **12** is more stable than **13** and **14** by 9.4 and 25.2 kcal mol^{-1}, respectively, indicating that the preferential bonding of 5-ethyl-2,2′-bipyridine with the Si(100) surface occurs with only one C atom and preserves the dimeric structure of the surface.

Coordination reaction with Cu^I ions: Contact-angle determinations can be used, in an ideal approximation, to estimate the surface free energy, γ_{total}, and its distinct components (the apolar Lifshitz–van der Waals, γ_{LW}, the Lewis electron acceptor or acid, γ_+, and the electron donor or basic, γ_-, components). Surface-energy values are collected in Table 2. On H−Si(100), the presence of a basic component is expected upon partial reoxidation of the substrate. The electron-acceptor portion of surface energy appears in all cases lower than its experimental error and should be considered to be negligible. The γ_{total} values strongly decrease upon Cu^I coordination to the CEG sample, mainly driven by γ_{LW}, whereas γ_- shows a relative maximum for the CEG sample.

After coordination of the CEG sample with Cu^I, statistical analysis of the AFM images from the related surface did not reveal a significant change in rms roughness (Figure 5d). XPS results on the same sample are reported in Figure 7a. A narrow Cu2p line shape is obtained, typical of Cu^I,[48] associated with a N:Cu atomic ratio of 4.0. These results were obtained for six independent samples. Two effects were found on the N1s peak after coordination: a narrowing of the peak width and a positive chemical shift of 0.5 eV (Figure 4). Reaction with Cu^I leaves the Si surface still low in oxide (Figure 4d).

In a reference experiment conducted by exposing hydrogen-terminated Si(100) to Cu^I ions dissolved in CH_3CN, copper uptake from the solution was evidenced, consistent with the literature.[70] However, the resulting energy positions for Cu2p and $CuL_3M_{4,5}M_{4,5}$ Auger lines are sizeably different from the CEG sample. The distinct cases represented by reaction of Cu^I with either hydrogen-terminated Si(100) or with the CEG sample are definitely confirmed by the corresponding values found for the Cu Auger parameter, which amount to 1849.3 and 1847.3 eV, respectively. Note that the analogous value for the unsupported [Cu(5-methyl-2,2′-bipyridine)$_2$]ClO_4 complex is 1847.6 eV, which coincides,

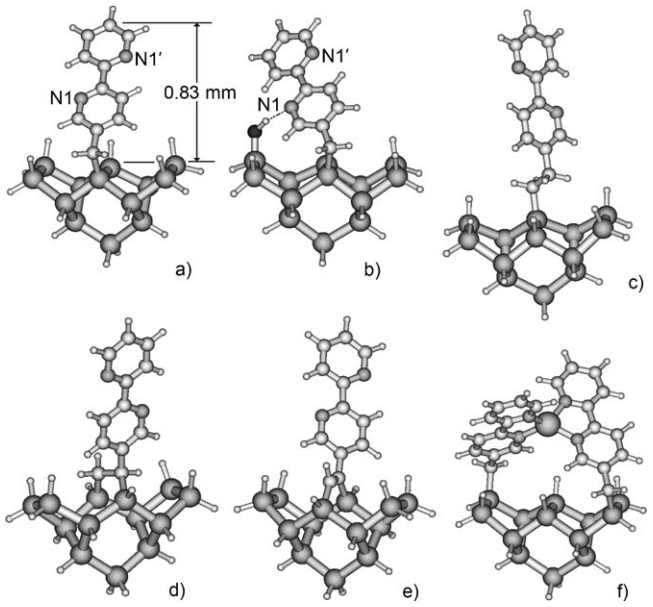

Figure 6. HF/3-21G optimized structures for: a) 5-methyl-2,2′-bipyridine bonded to monohydrogenated Si(100) (structure **1**, Table 3); b) 5-methyl-2,2′-bipyridine bound to monohydrogenated Si(100), in which a surface H atom is replaced by an OH group (structure **9**, Table 3); c) 5-ethyl-2,2′-bipyridine bonded to monohydrogenated Si(100) by the terminal ethyl C atom (structure **12**, Table 3); d) 5-ethyl-2,2′-bipyridine bound to monohydrogenated Si(100) by both ethyl C atoms (structure **13**, Table 3); e) 5-ethenyl-2,2′-bipyridine bonded to monohydrogenated Si(100) by both ethenyl C atoms and obtained by dehydrogenation of **13** (structure **14**, Table 3); f) $[Cu^{I}(SiCH_2\text{-}2,2'\text{-bipyridine})_2]^+$ complex bonded to monohydrogenated Si(100) (structure **15**, Table 3).

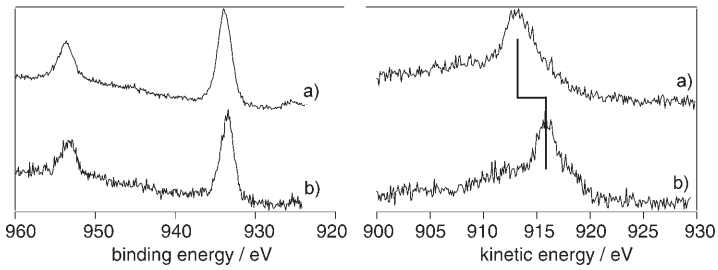

Figure 7. (Left) $Cu2p_{3/2,1/2}$ XPS spectra and (right) Cu Auger XPS spectra for hydrogen-terminated Si(100) samples after: a) electrografting of 5-bromomethyl-2,2′-bipyridine, followed by immersion in a 0.1 M solution of $[Cu(CH_3CN)_4]ClO_4$ in acetonitrile; b) immersion in a 0.1 M solution of $[Cu(CH_3CN)_4]ClO_4$ in acetonitrile.

within the experimental error (±0.2 eV), with the value for the CEG sample.

Figure 6f shows the optimized structure for $[Cu(Si\text{-}CH_2\text{-}2,2'\text{-bipyridine})_2]^+$ bonded to the monohydrogenated Si(100) surface. Surface coordination results in a slightly distorted tetrahedral geometry of Cu^{I}–N bonds, with nearly perpendicular 2,2′-bipyridine planes and Cu–N distances (0.195 nm) very close to those calculated for the free $[Cu(2,2'\text{-bipyridine})_2]^+$ complex. Although the resulting tetrahedral coordination is reasonable for a Cu^{I}–N_4 unit, the net atomic-charge analysis, performed by both Mulliken and DMA analysis, did not provide conclusive results upon Cu^{I} addition to the ligand.

Discussion

Clean, oxide-free, and flat hydrogen-terminated n- and p-Si(100) surfaces result from the preparation, as inferred from the AFM, contact-angle, and XPS results. On these surfaces 2,2′-bipyridine derivatives were successfully anchored by using the three different routes briefly summarized in Figure 1, although with distinctive features.

A quantitative comparison of the three series of samples can be made by taking into account molecular coverage, extent of Si oxidation, and level of contamination at the surface. The better compromise between higher extent of functionalization and lower Si oxidation can be clearly assessed from the results reported in Figure 3. For both n- and p-Si(100), an almost linearly decreasing trend in surface coverage as Si oxidation increases can be noted, the former series being more oxidized.[71] XPS Si intensity, however, does not differentiate between the surface being covered with silicon oxide or bipyridine. Therefore, the coverage values at high oxidation levels, deduced from XPS N/Si atomic ratios, are the more overestimated ones. In the region of the plot at which the coverage values are least affected by the formation of oxide, the CEG sample results as the better hybrid, which is also consistent with its C/N XPS atomic ratio, closer to the nominal value for the molecular moiety. In the comparison, the thermal approach leads to the formation of a greater amount of silicon oxide, probably because of the higher temperature of treatment, which activates the surface sites. Notice, however, that on porous Si, pyridine can catalyze the reaction of water to form silica.[72] This could justify the presence of silica in the three series of samples, probably induced by residual traces of water. The minimum amount of silica found for the CEG sample is consistent with the cathodic conditions applied, which renders it less susceptible to nucleophilic attack in water.[3]

An independent check for the quality of the CEG monolayer comes from its contact-angle values (Table 1), closely comparable to those for H–Si both before and, more remarkably, after Cu^{I} complexation. The modification induced by the stable presence of bipyridine at the surface in the CEG sample and the availability of its lone pairs is testified by the increase in surface hydrophilicity in water with respect to H–Si.[69] This is evidenced by the decrease in contact angle and the increase in the basic portion of the surface free energy with respect to H–Si. The resultant surface after complexation is more hydrophobic because nitrogen lone pairs are involved with Cu^{I} ions in the complex and do not interact with the solvent.

The notable hysteresis in advancing and receding contact angles exhibited by all monolayers in different solvents could indicate disorder because surface roughness and heterogeneity are not very relevant.[73] A major cause for disorder could be the different orientation of surface domains, which

prevents a two-dimensional dense packing of the molecules, allowing water to penetrate into the layer. The greater hysteresis found in polar versus apolar liquids could be assigned to a preferential interaction of polar liquids with silicon, and/or to the ability of the top layer to interact with polar groups through specific acid–base Lewis interactions.

The morphology of the CEG sample is inferred from analysis of AFM images, which show a submonolayer deposition pattern, with large ($20\times30\ nm^2$) assemblies. The mean value of height deduced from statistical analysis (0.82 nm) is practically coincident with the theoretical value for 5-methyl-2,2′-bipyridine grafted on a silicon surface (0.83 nm), as deduced from calculations and reported in Figure 6. These values are consistent with a monolayer deposition, and their distance from the average oxide thickness, deduced from XPS, excludes an assignment to patches of SiO_2.

XPS analysis, coupled with DFT calculations, allows the steps of surface functionalization and subsequent Cu complexation to be monitored.

The assignment of the secondary peak at ~401 eV, which accompanies the main pyridinic N1s component in the three series of samples, can be given on the basis of the following two main points:

1) In principle, a positive N1s chemical shift measured from the energy position of a neutral pyridinic N atom could be related to a monoprotonated bipyridine. A reference value of chemical shift that can assist in the assignment in the case of 2,2′-bypiridines is the energy distance between N1s in pyridinium and pyridine,[74] which amounts to 2 eV and parallels the theoretical difference in net charges of 0.5–0.6 a.u. found for the two species (Table 3). On this sole basis, the existence of protonated quaternary N atoms should be discarded in the present case.[75]
2) The presence of silanol groups from partial surface oxidation of Si is common, even in controlled conditions, because of the high reactivity of H–Si(100) with H_2O (Figure 6b). Hydrogen bonding between 2,2′-bipyridine and surface Si–OH groups (structures **9**–**11**) renders the interacting N atom more positive than the noninteracting one by 0.2–0.4 a.u. Such a charge difference is fully compatible with the (moderate) chemical shift of 1 eV.

On the basis of the above two points, the secondary N1s peak can be assigned to N atoms engaged in such hydrogen bonding.

The reaction of Cu^I with the CEG sample results in a Cu^I coordination complex with N-donor functions. On the basis of traditional solution chemistry of Cu^I with the bipyridine ligand, a 1:2 metal/ligand complex with tetrahedral geometry is expected. This is also found on the surface, as indicated by the 1:4 Cu/N atomic ratio given by XPS. The positive chemical shifts of the N1s peak related to N-ligand functions upon reaction with Cu^I strongly suggest the coordination of the N atoms to Cu^I ions. Furthermore, a tetrahedral $[Cu^I(bipyridine)_2]^+$ geometry for the complex on the Si(100) surface is supported by calculations (Figure 6f).

Notably, within the surface sensitivity of XPS, ~0.1 atomic %, all N atoms are engaged in the coordination bond to the Cu^I atom, in spite of their surface confinement. This may indicate that bipyridines are homogeneously bound and distributed on Si, and oriented in a way that allows the facile coupling of two ligands to a single Cu^I atom, with the correct tetrahedral geometry required by the cation. A possible contribution of acetonitrile in the coordination cannot be excluded, although the associated N1s binding energy cannot be confidently extracted from the literature. A partial participation of acetonitrile could account for the slight broadening of the N1s full width found upon coordination.

Results from AFM and dynamic contact-angle analysis give further, although less-direct, support to the extent of the surface-complexation reaction. In fact, in the CEG sample after coordination to Cu^I, a statistical analysis of AFM images indicates no sizeable change in rms roughness (Figure 5d). The good extent of surface-Cu^I complexation is also consistent with the much higher hydrophobicity of the complexed CEG hybrid, experimentally evidenced by dynamic contact angles greater than for the unreacted analogue.

Finally, Figure 6f shows a tentative structure for the surface complex formed by Cu^I with the CEG sample. The optimized geometry shows a slightly distorted-tetrahedral coordination of Cu^I, with nearly perpendicular 2,2′-bipyridine planes, and Cu–N distances (0.195 nm) very close to those calculated for the free $[Cu^I(2,2'\text{-bipyridine})_2]^+$ complex.

Further FTIR investigations are in progress to investigate the adsorption configurations in more detail.

Conclusion

A comparison study of the anchoring behavior of differently substituted 2,2′-bipyridine ligands was conducted on hydrogen-terminated Si(100). The formation of a covalent C–Si bond was evidenced by the characterization of the hybrids resulting from three different wet chemistry routes, employing thermal, photochemical, and electrochemical (CEG) approaches. Significant differences were observed in the corresponding hybrids, both in surface coverage and for the extent of silicon surface oxidation and contamination. The CEG route is the method of choice, because it represents the best compromise between the extent of Si functionalization, protection from substrate-oxidation reaction, and a low level of contamination. Additionally, it was shown that anchored bipyridine ligands, although confined on the surface, retain the same reactivity as a bidentate ligand towards Cu^I, as demonstrated by the formation of a 1:2 Cu–bipyridine complex on the surface, paralleling the known behavior in solution.

Acknowledgements

Università La Sapienza, Università di Pavia, and MIUR (Ministero dell'Istruzione, Università e Ricerca) PRIN projects, are thanked for financial support.

[1] A. B. Sieval, R. Linke, H. Zuilhof, E. J. R. Sudhölter, *Adv. Mater.* **2000**, *12*, 1457–1460.
[2] D. D. M. Wayner, R. A. Wolkow, *J. Chem. Soc. Perkin Trans. 2* **2002**, 23–34.
[3] J. M. Buriak, *Chem. Rev.* **2002**, *102*, 1271–1308.
[4] J. H. Song, M. J. Sailor, *Comments Inorg. Chem.* **1999**, *21*, 69–84.
[5] J. M. Buriak, *Chem. Commun.* **1999**, 1051–1052.
[6] R. J. Hamers, S. K. Coulter, M. D. Ellison, J. S. Hovis, D. F. Padowitz, M. P. Schwartz, C. M. Greenlief, J. N. Russell, Jr., *Acc. Chem. Res.* **2000**, *33*, 617–624.
[7] M. P. Stewart, J. M. Buriak, *Comments Inorg. Chem.* **2002**, *23*, 179–203.
[8] a) R. Zanoni, F. Cattaruzza, C. Coluzza, E. A. Dalchiele, F. Decker, G. Di Santo, A. Flamini, L. Funari, A. G. Marrani, *Surf. Sci.* **2005**, *575*, 260–272; b) R. Zanoni, A. Aurora, F. Cattaruzza, F. Decker, P. Fastiggi, V. Menichetti, P. Tagliatesta, A.-L. Capodilupo, A. Lembo, *Mater. Sci. Eng. C.*, DOI: 10.1016/j.msec.2006.07.014.
[9] K. Roth, A. A. Yasseri, Z. Liu, R. B. Dabke, V. Malinovskii, K. H. Schweikart, L. Yu, H. Tiznado, F. Zaera, J. S. Lindsey, W. G. Kuhr, D. F. Bocian, *J. Am. Chem. Soc.* **2003**, *125*, 505–517.
[10] Z. Liu, A. A. Yasseri, J. S. Lindsey, D. F. Bocian, *Science* **2003**, *302*, 1543–1545.
[11] L. Wei, D. Syomin, R. S. Loewe, J. S. Lindsey, F. Zaera, D. F. Bocian, *J. Phys. Chem. B* **2005**, *109*, 6323–6330.
[12] a) J. Bateman, R. D. Eagling, D. R. Worrall, B. R. Horrocks, A. Houlton, *Angew. Chem.* **1998**, *110*, 2829–2831; *Angew. Chem. Int. Ed.* **1998**, *37*, 2683–2685; b) T. Strother, W. Cai, X. Zhao, R. J. Hamers, L. M. Smith, *J. Am. Chem. Soc.* **2000**, *122*, 1205–1209; c) A. R. Pike, L. C. Ryder, B. R. Horrocks, W. Clegg, B. A. Connolly, A. Houlton, *Chem. Eur. J.* **2005**, *11*, 344–353; d) W. Liao, F. Wei, M. X. Qian, X. S. Zhao, *Sens. Actuators B* **2004**, *101*, 361–367; e) W. Feng, B. Miller, *Langmuir* **1999**, *15*, 3152–3156; f) D.-J. Guo, S.-J. Xiao, B. Xia, S. -Wei, J. Pei, Y. Pan, X.-Z. You, Z.-Z. Gu, Z. Lu, *J. Phys. Chem. B* **2005**, *109*, 20620–20628; g) A. R. Pike, S. N. Patole, N. C. Murray, T. Ilyas, B. A. Connolly, B. R. Horrocks, A. Houlton, *Adv. Mater.* **2003**, *15*, 254–257.
[13] D. Julthongpiput, Y. His-Lin, J. Teng, E. R. Zubarev, V. V. Tsukruk, *Langmuir* **2003**, *19*, 7832–7836.
[14] E. A. Dalchiele, A. Aurora, G. Bernardini, F. Cattaruzza, A. Flamini, P. Pallavicini, R. Zanoni, F. Decker, *J. Electroanal. Chem.* **2005**, *579*, 133–142.
[15] V. I. Boiadjiev, G. M. Brown, L. A. Pinnaduwage, G. Goretzki, P. V. Bonnesen, T. Thundat, *Langmuir* **2005**, *21*, 1139–1142.
[16] D. Xu, E. T. Kang, K. G. Neoh, Y. Zhang, A. A. O. Tay, S. S. Ang, M. C. Y. Lo, K. Vaidyanathan, *J. Phys. Chem. B* **2002**, *106*, 12508–12516.
[17] D. Xu, E. T. Kang, K. G. Neoh, A. A. O. Tay, *Langmuir* **2004**, *20*, 3324–3332.
[18] B. A. Sexton, N. R. Avery, *Surf. Sci.* **1983**, *129*, 21–36.
[19] A. Bansal, X. Li, I. Lauermann, N. S. Lewis, S. I. Yi, W. H. Weinberg, *J. Am. Chem. Soc.* **1996**, *118*, 7225–7226.
[20] S. Fellah, A. Teyssot, F. Ozanam, J.-N. Chazalviel, J. Vigneron, A. Etcheberry, *Langmuir* **2002**, *18*, 5851–5860.
[21] P. Allongue, C. H. de Villeneuve, J. Pinson, F. Ozanam, J.-N. Chazalviel, X. Wallart, *Electrochim. Acta* **1998**, *43*, 2791–2798.
[22] M. P. Stewart, F. Maya, D. V. Kosynkin, S. M. Dirk, J. J. Stapleton, C. L. McGuiness, D. L. Allara, J. M. Tour, *J. Am. Chem. Soc.* **2004**, *126*, 370–378.
[23] L. A. Zazzera, J. F. Evans, M. Deruelle, M. Tirrell, C. R. Kessel, P. J. Mckeown, *J. Electrochem. Soc.* **1997**, *144*, 2184–2189.
[24] M. R. Linford, C. E. D. Chidsey, *J. Am. Chem. Soc.* **1993**, *115*, 12631–12632.
[25] M. R. Linford, P. Fenter, P. M. Eisenberger, C. E. D. Chidsey, *J. Am. Chem. Soc.* **1995**, *117*, 3145–3155.
[26] C. Gurtner, A. W. Wun, M. J. Sailor, *Angew. Chem.* **1999**, *111*, 2132–2135; *Angew. Chem. Int. Ed.* **1999**, *38*, 1966–1968.
[27] R. Boukherroub, S. Morin, D. D. M. Wayner, F. Bensebaa, G. I. Sproule, J. M. Baribeau, D. J. Lockwood, *Chem. Mater.* **2001**, *13*, 2002–2011.
[28] P. Wagner, S. Nock, J. A. Spudich, W. D. Volkmuth, S. Chu, R. C. Cicero, C. P. Wade, M. R. Lindford, C. E. D. Chidsey, *J. Struct. Biol.* **1997**, *119*, 189–201.
[29] R. Boukherroub, D. D. M. Wayner, *J. Am. Chem. Soc.* **1999**, *121*, 11513–11515.
[30] C. J. Barrelet, D. B. Robinson, J. Cheng, T. P. Hunt, C. F. Quate, C. E. D. Chidsey, *Langmuir* **2001**, *17*, 3460–3465.
[31] J. M. Buriak, M. J. Allen, *J. Am. Chem. Soc.* **1998**, *120*, 1339–1340.
[32] J. M. Holland, M. P. Stewart, M. J. Allen, J. M. Buriak, *J. Solid State Chem.* **1999**, *147*, 251–258.
[33] J. M. Buriak, M. P. Stewart, T. W. Geders, M. J. Allen, H. C. Choi, J. Smith, D. Raftery, L. T. Canham, *J. Am. Chem. Soc.* **1999**, *121*, 11491–11502.
[34] A. Cricenti, G. Longo, M. Luce, R. Generosi, P. Perfetti, D. Vobornik, G. Margaritondo, P. Thielen, J. S. Sanghera, I. D. Aggarwal, J. K. Miller, N. H. Tolk, D. W. Piston, F. Cattaruzza, A. Flamini, T. Prosperi, A. Mezzi, *Surf. Sci.* **2003**, *544*, 51–57.
[35] F. Cattaruzza, A. Cricenti, A. Flamini, M. Girasole, G. Longo, A. Mezzi, T. Prosperi, *J. Mater. Chem.* **2004**, *14*, 1461–1468.
[36] G. F. Cerofolini, C. Galati, S. Reina, L. Renna, *Semicond. Sci. Technol.* **2003**, *18*, 423–429.
[37] M. P. Stewart, E. G. Robins, T. W. Geders, M. J. Allen, H. C. Choi, J. M. Buriak, *Phys. Status Solidi A* **2000**, *182*, 109–115.
[38] P. Hartig, J. Rappich, T. Dittrich, *Appl. Phys. Lett.* **2002**, *80*, 67–69.
[39] N. Shirat, T. Miura, K. Kobayashi, K. Koumoto, *Langmuir* **2003**, *19*, 9107–9109.
[40] F. Cattaruzza, A. Cricenti, A. Flamini, M. Girasole, G. Longo, T. Prosperi, G. Andreano, L. Cellai, E. Chirivino, *Nucleic Acids Res.* **2006**, *34*, e32.
[41] F. Cattaruzza, A. Flamini, D. Fiorani, P. Imperatori, G. Scavia, L. Suber, A. M. Testa, A. Mezzi, G. Ausanio, W. R. Plunkett, *Chem. Mater.* **2005**, *17*, 3311–3316.
[42] S. Palacin, C. Bureau, J. Charlier, G. Deniau, B. Mouanda, P. Viel, *ChemPhysChem* **2004**, *5*, 1468–1481.
[43] C. Kaes, A. Katz, M. Hosseini, *Chem. Rev.* **2000**, *100*, 3553–3590.
[44] V. Amendola, L. Fabbrizzi, P. Pallavicini, *Coord. Chem. Rev.* **2001**, *216*, 435–448.
[45] A. Aurora, M. Boiocchi, G. Dacarro, F. Foti, C. Mangano, P. Pallavicini, S. Patroni, A. Taglietti, R. Zanoni, Chem. Eur. J. **2006**, *12*, 5535–5546.
[46] J. Polin, E. Schmohel, V. Balzani *Synthesis* **1998**, *3*, 321–324.
[47] B. J. Hathaway, D. G. Holah, J. D. Postlethwaite, *J. Chem. Soc.* **1961**, 3215–3218.
[48] X. G. Zhang in *Electrochemistry of Silicon and Its Oxide*, Kluwer Academic, New York, **2001**.
[49] D. Briggs, M. P. Seah in *Practical Surface Analysis, Vol. I*, 2nd ed., Wiley, New York, **1990**.
[50] M. P. Seah, S. J. Spencer, *Surf. Interface Anal.* **2002**, *33*, 640–652.
[51] Gaussian 98 (Revision A.6), M. J. Frisch, G. W. Trucks, H. B. Schlegel, G. E. Scuseria, M. A. Robb, J. R. Cheeseman, V. G. Zakrzewski, J. A. Montgomery, Jr., R. E. Stratmann, J. C. Burant, S. Dapprich, J. M. Millam, A. D. Daniels, K. N. Kudin, M. C. Strain, O. Farkas, J. Tomasi, V. Barone, M. Cossi, R. Cammi, B. Mennucci, C. Pomelli, C. Adamo, S. Clifford, J. Ochterski, G. A. Petersson, P. Y. Ayala, Q. Cui, K. Morokuma, D. K. Malick, A. D. Rabuck, K. Raghavachari, J. B. Foresman, J. Cioslowski, J. V. Ortiz, B. B. Stefanov, G. Liu, A. Liashenko, P. Piskorz, I. Komaromi, R. Gomperts, R. L. Martin, D. J. Fox, T. Keith, M. A. Al-Laham, C. Y. Peng, A. Nanayakkara, C. Gonzalez, M. Challacombe, P. M. W. Gill, B. Johnson, W. Chen, M. W. Wong, J. L. Andres, C. Gonzalez, M. Head-Gordon, E. S. Replogle, J. A. Pople, Gaussian Inc., Pittsburgh, PA, **1998**.

[52] M. Szczesniak, K. Szczepaniak, J. S. Kwiatkowsky, K. KuBulat, W. B. Person, *J. Am. Chem. Soc.* **1988**, *110*, 8319–8330.
[53] A. Les, L. Adamowicz, R. J. Bartlett, *J. Phys. Chem.* **1989**, *93*, 4001–4005.
[54] R. S. Mulliken, *J. Chem. Phys.* **1955**, *23*, 1833–1840, 1841–1846, 2338–2342, 2343–2346.
[55] A. J. Stone, *Chem. Phys. Lett.* **1981**, *83*, 233–239.
[56] S. L. Price, A. J. Stone, M. Alderton, *Mol. Phys.* **1984**, *52*, 987–1001.
[57] G. Schaftenaar, J. H. Noordik, *J. Comput.-Aided Mol. Des.* **2000**, *14*, 123–134.
[58] C. J. van Oss, *Interfacial Forces in Aqueous Media*, Dekker, New York, **1994**.
[59] R. J. Good, C. J. van Oss in *Modern Approaches to Wettability* (Eds.: M. E. Schrader, G. I. Loeb), Plenum, New York, **1992**, pp. 1–28.
[60] C. Della Volpe, D. Maniglio, M. Brugnara, S. Siboni, M. Morra, *J. Colloid Interface Sci.* **2004**, *271*, 434–453.
[61] M. P. Seah, S. J. Spencer, *Surf. Interface Anal.* **2003**, *35*, 515–524.
[62] Y. Liu, S. Yamahazi, S. Yamabe, Y. Nakato, *J. Mater. Chem.* ***2005***, *15*, 4906–4913.
[63] M. P. Seah, W. A. Dench, *Surf. Interface Anal.* **1979**, *1*, 2–11.
[64] The inelastic-mean-free path for the monolayer was assumed to be equal to poly(4-vinylpyridine), reported in: P. J. Cumpson, *Surf. Interface Anal.* **2001**, *31*, 23–34.
[65] F. J. Himpsel, F. R. McFeely, A. Taleb-Ibrahimi, J. A. Yarmoff, *Phys. Rev. B* **1988**, *38*, 6084–6096.
[66] J. H. Scofield, *J. Electron Spectrosc. Relat. Phenom.* **1976**, *8*, 129–137.
[67] D. T. Clark, R. D. Chambers, D. Kilcast, W. K. R. Musgrave, *J. Chem. Soc. Faraday Trans. 2* **1972**, *68*, 309–319.
[68] X. Liu, K. G. Neoh, L. Zhao, E. T. Kang, *Langmuir* **2002**, *18*, 2914–2921.
[69] R. E. Johnson, R. H. Dettre, *J. Colloid Interface Sci.* **1977**, *62*, 205–212.
[70] S. Ye, T. Ichihara, K. Uosaki, *J. Electrochem. Soc.* **2001**, *148*, C421–C426, and references related to Si(100) reported therein.
[71] This effect could be due to the more likely occurrence of oxidation under light for the n-type, and/or to its high doping level employed here.
[72] G. Mattei, V. Valentini, V. A. Yakovlev, *Surf. Sci.* **2002**, *502–503*, 58–62.
[73] R. E. Johnson, Jr., R. H. Dettre, *Surf. Colloid Sci.* **1969**, *2*, 85.
[74] L. E. Cox, J. J. Jack, D. M. Hercules, *J. Am. Chem. Soc.* **1972**, *94*, 6575–6578.
[75] It should be recalled here that monoprotonated 2,2′-bipyridine exists as both *syn* and *anti* rotamers, and quantum chemical calculations on the two sets indicate a charge difference of ~0.6 a.u. between the N atoms of the first set (structures **4**–**5** in Table 3), but only 0.3–0.4 a.u. for the second set (structures **6**–**7**). This latter result could suggest that a chemical shift of 1 eV is representative of the presence of monoprotonated N atoms selectively in the *anti* rotamer structures. However, the latter structures are less stable than the *syn* forms by ~7 kcal mol^{-1}, and their occurrence on the Si(100) surface should be discarded for thermodynamic reasons.

Received: June 5, 2006
Published online: October 26, 2006

